Journal of Materials Chemistry C

Accepted Manuscript

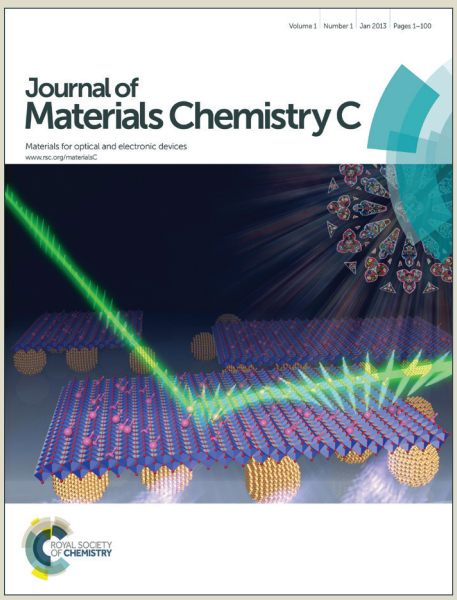

ROYAL SOCIETY OF CHEMISTRY

www.rsc.org/materialsC

Journal of Materials Chemistry C

ARTICLE

Can Hydrogen Bonds Improve the Hole-Mobility in Amorphous Organic Semiconductors? Experimental and Theoretical Insights

Received 00th January 20xx,
Accepted 00th January 20xx

DOI: 10.1039/x0xx00000x

www.rsc.org/

Viktorija Mimaite,[a] Juozas Vidas Grazulevicius,*[a] Rasa Laurinaviciute,[a] Dmytro Volyniuk,[a] Vygintas Jankauskas,[b] Gjergji Sini*[c]

Five hole-transporting triphenylamine derivatives containing methoxy and methyl groups are synthesized and investigated. The hole-mobility increases in the presence of methyl- and methoxy substituents, exceeding 10^{-2} cm^2/Vs in the case of the methyl groups. Quantum mechanical calculations on these compounds indicate very different dipole moments and intermolecular interaction strengths, with intriguing correlations to the trend in hole-mobility. Temperature dependent hole-mobility measurements indicate disorder dominated hole transport. The values of the energetic disorder parameter (σ) decrease upon methyl and methoxy substitutions despite the increase in dipole moments. This trend is discussed as a function of the interaction energy between adjacent molecules, the dipole moment, the molecular polarizability, and the conformational degree of freedom. Our results indicate that the global decrease of σ upon methyl and methoxy substitutions is dominated by the the larger decrease in the geometrical randomness component of the energetic disorder. A direct correlation is established between the decrease in geometrical randomness and the increase in intermolecular interaction energies, mainly stemming from the additional C-H….π,O,N hydrogen bonds induced by methyl and methoxy groups.

1. Introduction

Low-molar-mass semiconductors possess advantages against their polymer counterparts because of being easier to purify and characterize.[1] They are widely used in organic light-emitting diodes, organic photovoltaic devices, organic field-effect transistors.[2,3] The devices based on organic materials are attractive because they can take advantages of organic materials such as light weight, potentially low cost, and capability of thin-film, large-area, flexible device fabrication.[4] During the last years, much attention has been paid to derivatives of triphenylamine because of their good hole-transporting properties, making these materials promising candidates for optoelectronic and electronic devices.[5]

Photoelectrical and other properties of the derivatives of triphenylamine are considerably influenced by the nature and the number of the substituents. We focus here on the influence of methoxy- and methyl substituents. Methoxy substitutions have been found to enhance the dipole moment and decrease the charge mobility of substituted compounds as compared to the non-substituted ones.[6-8] However, recent studies[8-10] have reported on methoxy substituted compounds exhibiting larger hole-mobilities as compared to the non-substituted ones. The improvement of the hole-transporting properties upon methoxy substitutions has been suggested to partly stem from the (-C-H….π, N, O) hydrogen bonds established in the hole-transporting materials by means of methoxy groups.[9,10] While establishment of efficient C-H…π hydrogen bonds has been observed and studied in details by Nishio et. cooworkers since the late 70-ties,[11-13] their potential to impact the charge transport properties in organic semiconductors has been only recently reported.[9,10]

The contradictory effects of the methoxy substitutions on the hole-mobilities of amorphous materials[6-10] suggest consequently a subtle balance between effects playing in opposite directions. Static analysis in the frame of Marcus theory[14-16] was shown to give predictions in wrong agreement with the experimental results, suggesting dominating role of disorder effects.[9] Based on the well-established influence of the dipolar-moments on the energetic disorder,[6,7] methoxy substitutions are then expected to result in degraded- or improved charge transport properties, partly depending on the (respectively) important- or negligible increase of the molecular dipole moments. As will be shown in this study, the

[a] Department of Polymer Chemistry and Technology, Kaunas University of Technology, Radvilenu pl. 19, Kaunas, LT-50254, Lithuania. E-mail: juozas.grazulevicius@ktu.lt
[b] Department of Solid State Electronics, Vilnius University, Sauletekio al. 9, Vilnius, LT-10222, Lithuania.
[c] Laboratoire de Physicochimie des Polymères et des Interfaces, EA 2528 Université de Cergy-Pontoise, 5 mail Gay-Lussac, Cergy-Pontoise Cedex, 95031, France. E-mail: gjergji.sini@u-cergy.fr

Electronic Supplementary Information (ESI) available: Views of the unit cell, the optimized geometry of some selected model dimers and the two most strongly interacting dimers for compounds **4-8**. Experimental and theoretical absorption spectra for the compounds **4-8**. Data of the TOF measurement. Hole transport parameters for the layers of compounds **4-8**. Temperature dependent TOF results and analysis. Nature of intermolecular interactions. Cartesian coordinates (Å) of Dimer-6 for compounds **4-8**, optimized at the ωB97XD/6-31G(d,p) level in gas phase. See DOI: 10.1039/x0xx00000x

enhancement of the intermolecular interactions upon substitutions[9] will strongly interfere in the balance against the effects of the dipole-moment factor. One can thus imagine that, when designed judiciously, the addition of electronegative groups may avoid the negative effects of the increased dipole moments and the related increase in the energetic disorder. It is thus important to obtain more insight on the pros and cons of such substitutions, in order to provide additional guide-lines on molecular engineering.

In this study we focus on the effect of molecular-polarity modifications, resulting from the substitution of triphenylamine-twin compounds by methoxy and methyl groups. Unlike the methoxy substituted compounds reported in the literature, we show that in the case of triphenylamine-twin based compounds, important increase in the dipole moment is not necessarily synonym of decrease in charge mobility; enhancement of intramolecular interactions, recently reported in the literature,[9,10] will be shown to positively impact the hole mobility of these compounds.

2. Results

2.1. Synthesis

The synthetic routes to the compounds are illustrated in Scheme 1. The intermediates **1**-**3** were prepared by the modified Ullmann reaction between 4 4'-diaminobenzophenone and the corresponding aryl iodide. The target compounds **4**-**8** were obtained by Wittig-Horner method using the synthesized triphenylamine-based ketones and different benzylphosphonates. All the reactions were controlled by thin layer chromatography (TLC). The synthesized compounds were purified by column chromatography and isolated as yellow solids. Their chemical structures were confirmed with infrared- (IR), proton and carbon nuclear magnetic resonance- (^{1}H NMR and ^{13}C NMR) spectroscopies and mass spectrometry. The target compounds **4**-**8** were also characterized by elemental analysis.

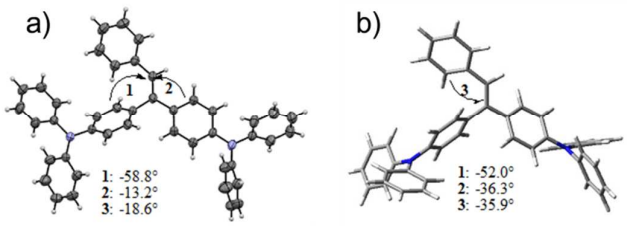

Fig. 1 (a) X-ray ORTEP structure of compound **4** and (b) the corresponding optimized geometry obtained at the ωB97XD/6-31G(d,p) level (in the absence of medium effect).

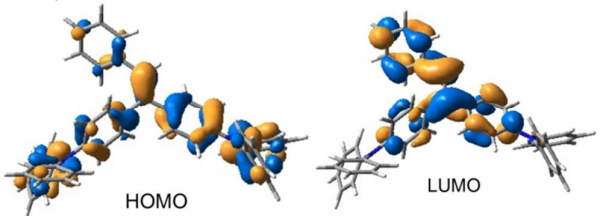

Fig. 2 HOMO and LUMO pictograms of compound **4**.

Absorption bands of C=O group observed in the IR spectra of compounds **1**-**3** at 1643-1647 cm^{-1} disappear in the spectra of compounds **4**-**8**. The proton signals of methoxy and methyl groups of synthesized products **5**-**8** in the ^{1}H NMR spectra are observed approximately at 3.80 and 2.30 ppm, respectively. Mass spectra of all the synthesized compounds show the corresponding molecular ion peaks. A crystal structure was obtained in the case of compound **4**, and the corresponding oak ridge thermal ellipsoid plot (ORTEP) view is given in Fig. 1 and Fig. S1.

2.2. Geometries and frontier orbitals of isolated molecules

The X-ray and theoretical geometries of compound **4** (non-substituted) are presented in Fig. 1, both exhibiting similar global shape. A limited selection of dihedral angles is also shown, indicating globally smaller experimental phenyl-ethenyl dihedral angles than the theoretical ones. These differences are due to the crystal-packing forces, as can be seen from the molecular overlap pattern in Fig. S1, which are absent during the theoretical geometry optimizations on isolated molecules. Similar observations and comments apply to the dihedral angles around the nitrogen atoms.

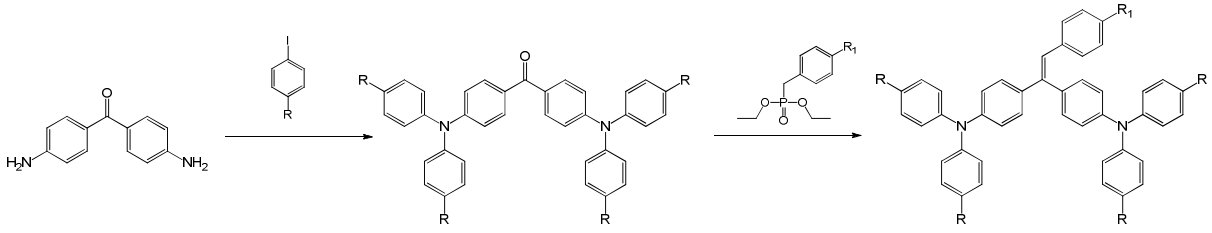

	1	2	3	4	5	6	7	8
R	H	OCH_3	CH_3	H	OCH_3	OCH_3	CH_3	CH_3
R_1	-	-	-	H	H	OCH_3	H	CH_3

Scheme 1 Synthesis of compounds **4**-**8**.

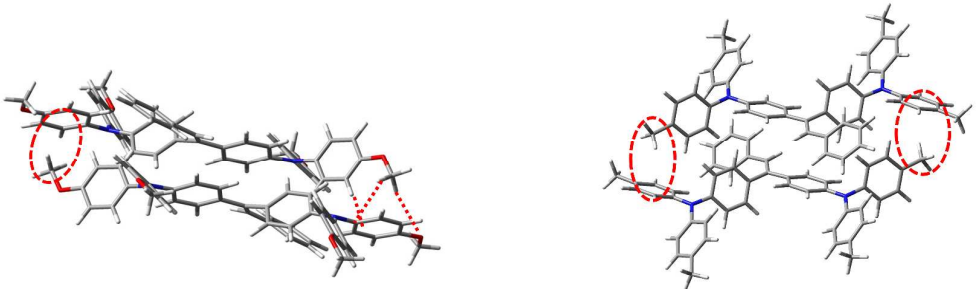

Fig. 3 Example of dimers constituted by two identical molecules in the case of compounds **5** (left) and **7** (right). The CH_3….π(Ph) and CH_3….O H-bonds established by means of methyl and methoxy groups are highlighted by red dashed lines or circles. See Fig. S2 for more examples.

These general geometric features remain basically the same upon methoxy and methyl substitutions (compounds **5** or **6**, and **7** or **8** respectively).

HOMO and LUMO of the non-substituted compound **4** are basically localized on the triphenylamine (TPA) and phenyl-ethenyl moieties respectively (Fig. 2). The methoxy and methyl substitutions on the TPA moieties are consequently expected to impact more importantly the HOMO energies as compared to LUMO ones. An opposite observation applies to *para*-phenyl-ethenyl substitutions, explaining the higher LUMO energy of **6** (methoxy substituens on all phenyl groups) as compared to compound **5** containing no substitution on phenyl-ethenyl moiety (Table S1).

2.3. Role of substituents on the intermolecular interactions: impact of hydrogen bonds

In order to obtain some insight on the impact of methoxy and methyl substitutions in the condensed phase of compounds **4**-**8**, six model dimers were optimized for each of compounds **4**-**8** (Fig. 3 and Fig. S2), and the dissociation energies and the average intermolecular distances were calculated. The results of these calculations are given in Table 1 and Tables S2, S3, and S4. The important result is that *the intermolecular interactions are strengthened upon methoxy and methyl substitutions* (**4** < **7** < **8** < **5** < **6**), from 15.4 kcal/mol for compound **4** to 17.6-20.4 kcal/mol for **5**-**8**.

In order to understand the factors influencing the strengthening of intermolecular interactions upon methoxy and methyl substitutions (by up to 4-5 kcal/mol), we try to obtain deeper insight on the nature of intermolecular interactions in solid films of these compounds.

An extensive geometrical and energetic analysis on the origin of the intermolecular interaction energy in compounds **4**-**8** is given in Annex I (SI), so that only the basic conclusions will be given here: (i) several (-C-H….π, O) hydrogen bonds (H-bonds) are established in compounds **4**-**8**. (ii) The attractive interaction in the non-substituted compound **4** stems from the dispersion and electrostatic contributions in π-π stacked moieties and the (Ph)C-H….π H-bonds. (iii) The increasing interaction energies (IE) by up to 4-5 kcal/mol in the order **4** < **7** < **8** ≈ **5** < **6** are principally (~60-70%) due to the additional CH_3….π(Ph) and CH_3….O H-bonds established by means of methyl and methoxy groups (Fig. 3). (iv) The trend in IE across the series is explained by the stronger H-bonds established by the methoxy groups as compared to the methyl ones (compounds **5**-**6** as compared to **7**-**8**) and by the number of the H-bonded groups (three groups for **6** and **8**, versus two for **5** and **7**). This last conclusion is comforted by recent experimental evidence reporting on increasing IE with increasing number of H-bonds in polyurethane/phenol mixtures.[17]

Table 1 Average dissociation energies (ΔE_D) calculated from selected dimers of model compounds **4**-**8** (in "gas phase"), average intermolecular distance between adjacent molecules (*d*), calculated at the ωB97X-D/6-31G(d,p) level (ZPE and BSSE corrected), and thermal characteristics of compounds **4**-**8**. Individual values of parameters ΔE_D, and d for each dimer and each compound are given in Tables S3, and S4.

Compound	ΔE_D [a] [kcal/mol]	d [a] [Å]	$T_{deg\text{-}5\%}$ [°C]	T_m [°C]	T_g [°C]
4 (H,H)	15.4	3.92 (5.72)	426	160	77
5 (OMe,H)	18.9	3.84 (5.87)	434	181	76.5
6 (OMe,OMe)	20.4	3.82 (5.81)	436	-	74
7 (Me,H)	17.6	3.88 (5.99)	429	-	71
8 (Me,Me)	19.0	3.85 (6.01)	430	-	73

[a] Average values, calculated over six different dimer isomers for each compound. The d values in parenthesis correspond to the average intermolecular distances calculated over all atoms of the molecules, whereas the smaller values correspond to the average intermolecular distances calculated between the overlapping molecular fragments only. $T_{deg\text{-}5\%}$ - 5% weight loss temperature, T_m - melting point, T_g - glass transition temperature was determined from second heating scan.

2.4. Thermal properties

The thermal characteristics of synthesized compounds were investigated by differential scanning calorimetry (DSC) and thermogravimetric analysis (TGA) under a nitrogen atmosphere. The data are summarized in Table 1. All the derivatives demonstrate high thermal stability. The $T_{deg\text{-}5\%}$ values of compounds **4**-**8** are comparable and range from 426 to 436°C, which is in good agreement with the increase of interaction energies in the same order (Fig. 4). The

investigations revealed that compounds **4** and **5** can exist both in crystalline and amorphous state. Derivatives **4** and **5** were obtained as crystalline materials. In the first DSC heating scan they showed endothermic melting signals at 160 and 181°C, respectively, again supporting the stronger intermolecular interactions calculated for compound **5** as compared to **4**. The cooling and second heating scans revealed only a glass transition of 77°C for both the compounds. Fig. 5a shows DSC heating and cooling curves for compound **4**. Compounds **6** and **8** were isolated as amorphous materials and exhibited only glass transitions at 74 and 73 °C in the first and the following DSC scans. Neither melting nor crystallization signals were observed in the DSC curves. As an example the DSC curves of compound **6** are shown in Fig. 5b.

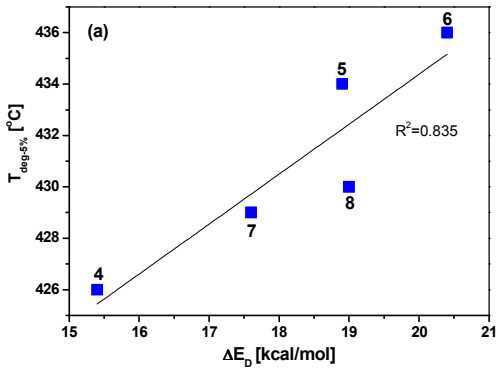

Fig. 4 Temperature of 5% weight loss of compounds **4-8** parametric on the average interaction energy.

2.5. Optical properties

The experimental and theoretical absorption spectra of compounds **4**, **5** and **7** are shown in Fig. 6 and Fig. S3 respectively, whereas the corresponding λ_{ab} wavelengths are collected in Table 2.

Compounds **4**-**8** exhibit absorption bands in the wavelength range from 200 to 425 nm. Theoretical absorption spectra (Fig. S3-4) and the HOMO and LUMO plots (Fig. 2 and Fig. S4) indicate that the absorption bands located around 300 nm can be attributed to the local TPA→TPA $\pi \rightarrow \pi^*$ electronic transitions. The absorption band around 350 nm are due to HOMO-1,HOMO→LUMO transitions, basically corresponding to a transition from a mixture of extended TPA-ethenyl π-electron orbitals toward the antibonding π^* orbital of the ethenyl fragment. Some charge-transfer character is consequently associated to the low-energy band. The maxima of the lowest energy absorption bands of compounds **5**-**7** having electron-donating methyl- or methoxy substituents are slightly red shifted with respect to that of compound **4** without substituents, which is basically due to the decreasing HOMO-LUMO gap (Table S1) with increasing σ - and π donor effect in the order H < CH_3 < OCH_3.

The effect of the substituents on the fluorescence spectra in tetrahydrofuran is more tangible, suggesting increased dipole moments in the 1st excited state for all compounds.

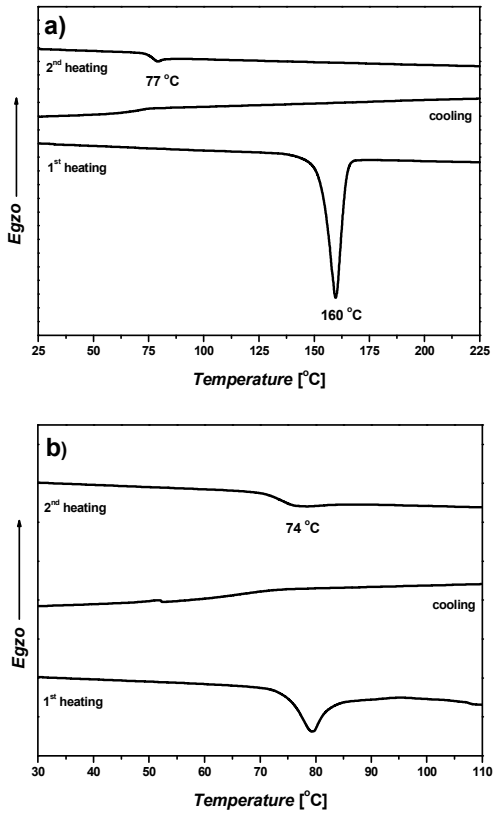

Fig. 5 DSC curves of compound **4 (a)** and **6 (b)**.

The Stokes shifts are larger for compounds **5** and **6** (140 nm and 130 nm respectively, Table 2) as compared to **7** (116 nm) and **4** (101 nm). This seems to principally translate the decreasing of the solvent-relaxation contribution in the 1st excited state, which is consistent with the trend in the 1st excited state dipole moment (see computational details), varying in the order **5** (6.4 D) > **6** (4.5 D) > **7** (3.9 D) > **4** (3.0 D). The larger Stokes shift of **8** (113 nm) as compared to **4** (101 nm), exhibiting identical excited state dipole moments (3.0 D), points to the role of the geometry relaxations of the additional chemical bonds in the excited state of substituted compounds as compared to the non-substituted one.

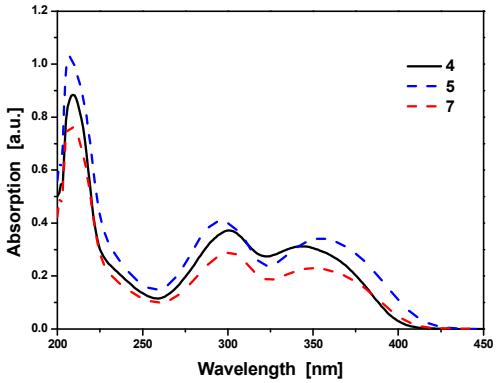

Fig. 6 Absorption spectra of dilute tetrahydrofuran solutions of compounds **4**, **5** and **7**.

Table 2 Electrochemical, optical and photoelectrical characteristics of compounds **4**-**8.** The theoretical absorption $S_0 \rightarrow S_1$ values, the experimental Stokes shifts, and the theoretical adiabatical IP values are given in parentheses. Theoretical adiabatic IP values were calculated at the B3LYP/6-31G(d,p) level in gas phase.

Compound	Electrochemical[a]					Photoelectrical		Optical	
	E_{ox1}, [V]	E_{onset} [V]	E_g^{opt} [eV]	IP_{SS} [eV]	EA_{SS} [eV]	IP_{PE} [eV]	ε_{HOMO} [eV]	λ_{ab} [nm]	λ_{fl} [nm]
4 (H,H)	0.63	0.54	3.08	5.19	2.11	5.56 (5.68)	-4.85	209, 301, 344 (380)	445 (101)
5 (OMe,H)	0.41	0.33	2.99	4.98	1.99	5.25 (5.33)	-4.52	207, 295, 355 (404)	495 (140)
6 (OMe,OMe)	0.39	0.31	3.01	4.96	1.95	5.23 (5.22)	-4.43	207, 298, 352 (398)	482 (130)
7 (Me,H)	0.53	0.45	3.03	5.10	2.07	5.40 (5.53)	-4.70	208, 301, 350 (396)	466 (116)
8 (Me,Me)	0.51	0.43	3.04	5.08	2.04	5.35 (5.35)	-4.66	209, 302, 348 (396)	461 (113)

[a] Electrochemical calculation were carried out according formulas: $E_g^{opt} = 1240/\lambda_{onset}$, $IP_{SS} = 4.8 + E_{onset}$, $EA_{SS} = IP_{SS} - E_g^{opt}$.

Compounds **5**-**8** exhibit blue fluorescence with fluorescence intensity maxima being in the range from 461 to 495 nm, as compared to 445 nm for compound **4**.

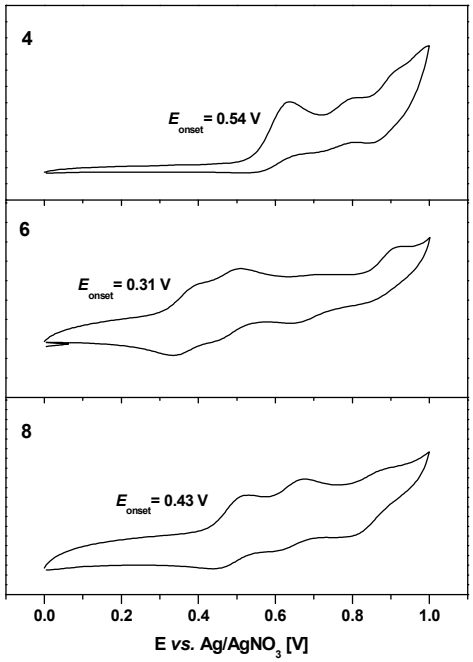

Fig. 7 Cyclic voltammograms of compounds **4**, **6** and **8** at a scan rate of 50 mVs^{-1}.

2.6. Electrochemical and photoelectrical characteristics

The electrochemical and photoelectrical characteristics of compounds **4**-**8** are presented in Table 2. Theoretical adiabatic ionization potential (IP) values, calculated at the B3LYP/6-31G(d,p) level in gas phase, are given in parentheses. The cyclic voltammetry (CV) was used to estimate electrochemical behaviour of compounds **4**-**8**. The cyclic voltamperograms of **4**, **6** and **8** are shown in Fig. **7**.

Electrochemical investigation of the solutions of compounds **4**-**8** in dichloromethane revealed that oxidative processes started at 0.63, 0.41, 0.39, 0.53 and 0.51 V, respectively. The onset values were estimated from the first oxidation event by taking the intersection between the baseline and the tangent line drawn to the increasing part of the current. The solid state ionization potentials (IP_{SS}) were calculated from the onset potentials after calibration of the measurements against Fc/Fc^+. The IP_{SS} values range in a very small window of 4.96-5.19 eV. Incorporation of methoxy and methyl groups in to the structures of triphenylamine-twin compounds leads to a decrease of IP_{SS} by *ca*. 0.2 and 0.1 eV, respectively (*cf*. IP_{SS} of **4** with those of **5**-**8**). The electron affinities (EA_{SS}) were obtained from the IP_{CV} values and the optical band gaps, which were deduced from the edges of the absorption spectra. The EA_{SS} values of **4**-**8** were found to be in the range from 1.95 to 2.11 eV.

The ionization potentials (IP_{PE}) of the amorphous films of compounds **4**-**8** were also estimated by electron photoemission technique. They were found to spread over a larger range (5.23 to 5.56 eV) as compared to the IP_{SS} values. The difference between IP_{SS} and IP_{PE} values is apparently due to the different polarisation (environments) in dilute solutions and solid layers of the compounds. However, IP_{PE}, IP_{SS}, and the theoretical IP values as well (Table 2), provide similar trends (**4** > **7** > **8** > **5** > **6**), which is consistent with the trend of the HOMO energies. This trend can be explained by the σ- and π donor effect of methyl and methoxy groups respectively: while the σ donor effect of methyl groups increases from **7** to **8** (increasing number of methyl groups), the strong π donor effect of methoxy groups increases with the number of substituents in the molecules, explaining the increasing HOMO energy from **5** to **6**.

2.7. Hole-transport characteristics

The room temperature electric field dependencies of hole-drift mobility for the films of compounds **4**-**8** are presented in Fig. 8. Compounds **7** and **8** having methyl substituents exhibited better charge-transporting properties than the corresponding derivatives **5** and **6** having methoxy substituents, in turn presenting only slightly higher hole-mobility as compared to the parent non-substituted compound **4**. Hole-drift mobility of *ca*. $1.5 \cdot 10^{-2}$ cm^2/Vs were recorded in the layers of **7** and **8** at an

electric field of $3.6 \cdot 10^5$ V/cm, which are very high values as for disordered organic materials.

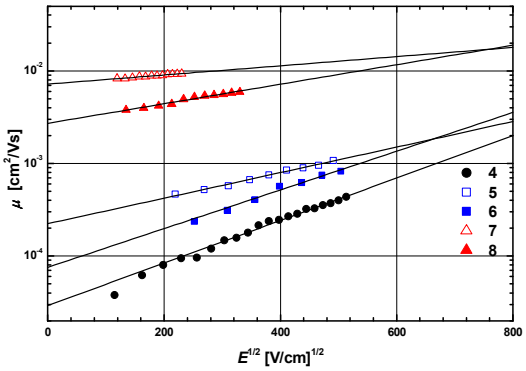

Fig. 8 TOF electric field dependencies of hole-drift mobility in the layers of compounds **4**-**8**.

The similarity in hole-transport properties of non-substituted and methoxy-substituted compounds is very intriguing, given the important electronic modifications induced by the methoxy groups. Similarly, the higher hole-mobility by roughly one order of magnitude of methyl substituted compounds **7** and **8** as compared to the methoxy substituted ones is also very interesting to unveil.

Intrinsic electronic properties. In order to obtain some insight on the factors influencing the hole mobility in these compounds, different electronic and charge transfer properties for the isolated molecules were calculated. Additionally, the HOMO-HOMO electronic couplings were calculated for the six model dimers optimized for each compounds **4**-**8** (Fig. 3 and Fig. S2).

The results of these calculations (Tables 1, 3 and Tables S2-S4) are intriguing. Globally, the intramolecular reorganization energies and the average HOMO-HOMO electronic couplings for compounds **4**-**8** range in small windows (0.13-0.20 eV and 0.005-0.015 eV respectively, Table 3), thus suggesting small variations in hole-mobility across the series. However, several discrepancies can be observed. Indeed, the best hole-transporting compound **7** presents the lowest electronic coupling values, whereas the best combination of the lowest intramolecular reorganization energy and almost the highest electronic coupling corresponds to compound **5** (0.129 eV and 0.014 eV respectively), for which a smaller hole mobility by one order of magnitude as compared to **7** is measured. Additionally, important differences between these compounds concern the correlation of hole-mobilities with the dipole moments and the interaction energies: (i) the dipole moments differ by up to 2-3 D (**4** < **7** < **8** < **5** < **6**, Table 3). The increase in dipole moments by roughly 3 D between **4** and **5**-**6** suggests important decreasing hole-mobilities in the same order,[18] which is in opposite agreement with the experimental observations ($\mu_4 < \mu_6 < \mu_5 < \mu_8 < \mu_7$). (ii) The intermolecular dissociation energies differ by up to 4.3 kcal·mol^{-1} across the series (**4** < **7** < **8** < **5** < **6,** Table 1). Accordingly, very different hole-mobilities would be expected, which is at odds with the very similar hole-mobilities measured for the strongest and weakest interacting compounds **5**-**6** and **4** respectively (Fig. 8).

Table 3 TOF hole-mobilities at $3.6 \cdot 10^5$ V/cm measured on vacuum-evaporated films of compounds **4**-**8**, intramolecular reorganization energies (λ_i), HOMO-HOMO electronic couplings (t), dipole moments (p), and static isotropic polarisabilities (α). All parameters were calculated at the B3LYP/6-31(d,p) level. Individual values of the parameter t for each dimer and each compound are given in Tables S2.

Compound	μ [cm^2/Vs]	λ_i [eV]	t^a [eV]	p [D]	α^b [bohr^3]
4 (H,H)	$7 \cdot 10^{-4}$	0.201	0.012	0.8	506 (504)
5 (OMe,H)	$1.7 \cdot 10^{-3}$	0.129	0.014	0.8-3.8 (2.8)	587 (524)
6 (OMe,OMe)	$1.4 \cdot 10^{-3}$	0.184	0.015	1.1-3.3 (2.2)	610 (532)
7 (Me,H)	$1.5 \cdot 10^{-2}$	0.145	0.004	1.4	566 (516)
8 (Me,Me)	$1.2 \cdot 10^{-2}$	0.172	0.010	1.3	582 (519)

[a] Average values, calculated over six different dimer isomers for each compound. [b] In parentheses are shown isotropic polarisability of the core-compounds (corresponding to the same number of electrons for each compound), estimated by subtracting the contribution of the substituents (R=H, CH_3, OCH_3) from the total polarizability values.

Determination of disorder parameters. Temperature dependent mobility measurements on vacuum evaporated films of compounds **4**-**8** were consequently conducted. The energetic disorder parameter (σ, Table 4) was deduced within the Gaussian disorder model, according to the following equation:[19]

$$\mu = \mu_0 \exp[-(\frac{2\hat{\sigma}}{3})^2] \exp[C(\hat{\sigma}^2 - \Sigma^2)E^{1/2}] \quad (1)$$

Here, σ is the energy width of the hopping site manifold, Σ is the positional disorder, C is a constant, and $\hat{\sigma} = \sigma/kT$.

Details on the method[7] and the results of all measurements are given in the SI (Annex II, Fig. S5-S8, and Table S5). The important result is that the values of the energetic disorder parameter σ decrease importantly from 0.145 eV to 0.087 eV in the order **4** > **5** = **6** > **8** > **7** (Table 3 and Fig. 9), which is consistent with the increasing of hole-mobilities in the same order. Large mobility prefactor values (μ_0, Table S5) in the range 1.5-40.9 cm^2/Vs were obtained for these compounds (**7** < **8** ≈ **6** < **4** ≈ **5**), suggesting interesting intrinsic hole transport properties for these compounds. However, the highest μ_0 value found for **4** and the smallest one found for **7** are, again, at odds with respect to the opposite trend of the field-dependent hole-mobilities at room temperature. These out of trend experimental μ_0 values and the out of trend combinations of intrinsic parameters discussed earlier in this section, suggest that the differences in the hole-mobilities of compounds **4**-**8** are dominanted by disorder phenomena.

Intriguingly, the decreasing σ values across the series are in opposite agreement with the important increase of dipole moments in the same order. The role of the dipole moment and interaction energy factors on the energetic disorder parameter σ need consequently to be analysed in more details, which is the focus of the following section.

3. Discussion

In terms of disorder models,[19] the increasing width of the energetic-disorder distribution (σ) of the states involved in the charge-transport impacts negatively the charge mobility. Following Borsenberger et al.[18] and limiting the discussion to the case of pure films (our case), we express σ as a sum of two contributions:[18]

$$\sigma^2 = \sigma_{dip}^2 + \sigma_{vdW}^2 \quad (2)$$

The first term is related to the fluctuations in electrostatic potential due to charge-dipole interactions, and is proportional to the dipole moment of the molecules. The second term, called the van der Waals term, is related to fluctuations of the electrostatic potential stemming from charge- induced dipole interactions and other permanent- and/or induced dipole-dipole interactions. In the case of tri-*p*-tolylamine (TTA)[18] or TPA[6] doped polymers, the parameter σ_{vdW} has been shown to increase with the increasing distance between the molecules (decreasing TTA or TPA concentration), possibly due to the increase in structural randomness.

3.1 Estimation of σ_{dip} and σ_{vdW}

The last correlation between σ_{vdW} and the distance between molecules suggests a direct qualitative relation between the dipole moments, intermolecular interaction strength, and σ_{vdW} parameter: increasing of molecular dipole moments (by means of methyl and methoxy substitutions) results, admittedly, in increasing σ_{dip} contributions, but is additionally expected to result in enhanced intermolecular interactions and reduced intermolecular distance, hence in decreased σ_{vdW} values. In order to get some insight on the balance between these two opposite effects in compounds **4**-**8**, the σ_{dip} values were evaluated by using Dieckmann's[20] and Yang's[21] relation (Equation 3, computation methodology), and the σ_{vdW} values were deduced from Equation 2. Note that the determination of σ_{vdW} values is not independent, however the trends observed on these values allow for physically meaningful comments.

The absolute values of σ, σ_{dip}, σ_{vdW} across the series of compounds **4**-**8** are given Table 4, whereas their evolutions are shown in Fig. 9. The σ_{dip} values principally depend on the dipole moments and the intermolecular distances (Equation 3, computation methodology). Given the negligible variations of intermolecular distances across the series of compounds **4**-**8** (5.72-6.01 Å), the differences in σ_{dip} values in Fig. 9 translate differences in dipole moments by up to 2-3 D in the order **4** < **8** < **7** < **6** < **5** (Table 4). However, *the contribution of σ_{dip} to the total σ is found to be of minor importance* (3-39%, Table 4). Note that, while the σ_{dip} values in Table 4 should be considered as qualitative ones, the global decrease of the total σ implies that the increase in σ_{dip} in the order **4** < **7**,**8** < **5**,**6** is overcompensated by a larger decrease in σ_{vdW} in the same order. The pertinent information to retain at this point is that (i) *σ_{vdW} is the dominant contribution to the total σ* of compounds **4**-**8** (ii) both total *σ and σ_{vdW} decrease upon methyl and methoxy substitutions*. In the following we focus on the evolution of σ and σ_{vdW} across the series.

Table 4 Energetic disorder parameter (σ), dipole component (σ_{dip}), van der Waals component (σ_{vdW}) values and the corresponding square values, percentage of σ^2_{dip} with respect to σ^2 values for each compound, and number of additional conformers associated with the presence of methyl or methoxy groups (N). The percentage of σ^2_{vdW} values of compounds **5-8** with respect to σ^2_{vdW} value of compound **4** are given in parentheses.

Compound	σ [eV]	σ_{dip} [a] [eV]	σ_{vdW} [b] [eV]	σ^2 $[eV]^2$	σ^2_{dip} $[eV]^2$	% σ^2_{dip}	σ^2_{vdW} $[eV]^2$	N [c]
4 (H,H)	0.145	0.025	0.143	0.021	0.001	3	0.020	-
5 (OMe,H)	0.133	0.083	0.104	0.018	0.007	39	0.011 (-47%)	256
6 (OMe,OMe)	0.133	0.067	0.115	0.018	0.004	25	0.013 (-35%)	1024
7 (Me,H)	0.087	0.040	0.077	0.008	0.002	21	0.006 (-71%)	16
8 (Me,Me)	0.110	0.037	0.104	0.012	0.001	11	0.011(-47%)	32

[a] Calculated from Equation 2. [b] Calculated from Equation 1.[c] Calculated according to the formula: $N=(n_{C\text{-}C}*n_{C\text{-}O})^{Ns}$, with $n_{C\text{-}C}$= 2 being the number of conformations corresponding to a methyl group, $n_{C\text{-}O}$= 2 being the number of OMe conformations with respect to a C(phenyl)-O(methoxy) bond, and Ns being the number of substituents.

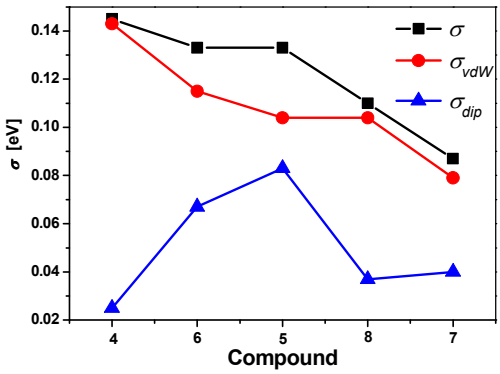

Fig. 9 Evolution of the total energetic disorder parameter σ, dipolar component σ_{dip}, and the van der Waals component σ_{vdW}, across the series of compounds **4**-**8.** The σ_{vdW} values are calculated by means of Equation 2. The ordering of the compounds in the abscissa follows that of the increasing hole-mobilities. The lines in the figure have no physical meaning, and are only guides for the eye.

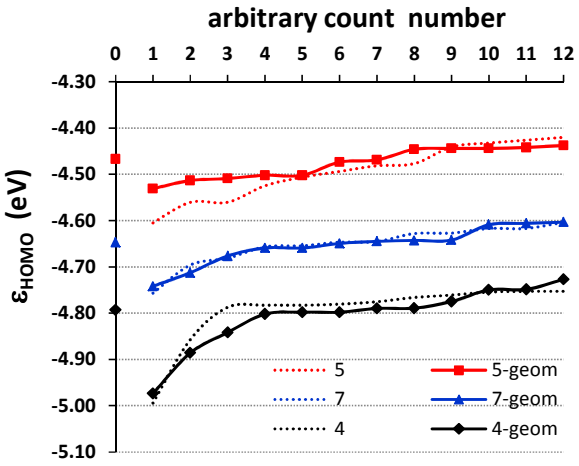

Fig. 10 HOMO energy for each fragment in the six dimer types of compounds **4**, **5**, and **7**, calculated by two methods: for a given dimer, each fragment taken at the dimer geometry is calculated either isolated (plain lines), or in the presence of the second dimer (dashed lines). The numbers in the abscissa are meaningless and correspond to the ordering of fragments of each plot in the increasing order of HOMO energies. Point zero corresponds to the HOMO energy in the geometry of the isolated compounds. The lines in the figure are only guides for the eye.

3.2 Impact of the intermolecular interaction energy (IE) on the geometrical randomness.

The influence of methoxy and methyl substitutions on the σ and σ_{vdW} values convolutes several mechanisms. In this section we focus on the geometrical randomness at the molecular level only, which is in direct correlation with the IE factor. Indeed, in the case of non-rigid molecules containing more or less freely rotating substituents, random packing patterns in amorphous films induce variations in molecular geometry that enlarge the distribution of the HOMO energies, thus increasing the width of the density of states (DOS).[22] This last contribution to the energetic disorder is of "intramolecular" nature, thus being in direct correlation with the strength of the intermolecular interactions. Note that we ignore here the impact of the IE factor on the intermolecular structural randomness (in distances and orientations). Other factors, including electrostatic and van der Waals polarizations, intrinsic molecular polarizability, and conformational freedom, will be treated in the following sections.

As a means to check for the effect of the IE factor, we have calculated the distribution of the HOMO energies over a selected number of packing patterns. These "solid-phase" geometries were obtained by optimizing six dimer types for each compound **4**-**8** (section 2.3). We have consequently obtained a small "random" distribution of twelve molecular fragment geometries for each compound. By calculating the HOMO energy of each isolated fragment at the geometry of the optimized dimers, we obtain a distribution of twelve energy values for each compound. Given that we have optimized identical dimer types for each compound, the comparison between HOMO-energy distributions of different compounds remains pertinent. The trend in energy distributions of different compounds can thus give a good estimation for the trends in the corresponding disorder parameters. Note that while relying on a very small sampling (twelve molecular geometries for each compound), the results remain pertinent as the sampling covers very different dimer types, with interaction energies varying by 2-3 times (Table S3).

In order to consider a homogeneous series of compounds and avoid interference with other factors, we firstly compare only compounds **4**, **5**, and **7**. The "solid-phase" HOMO energies corresponding to each fragment and for each compound are plotted in Fig. 10 (plain lines), whereas the widths of their HOMO-energy distributions (difference between maximum and minimum values) and the corresponding standard deviations are collected in Table 5. The "gas phase" HOMO energies corresponding to the non-deformed geometries of the isolated compounds **4**, **5**, and **7** are also shown (zero-point in abscissa).

Fig. 10 indicates that roughly half of the calculated "solid-phase" fragments exhibit higher HOMO levels as compared to the "gas-phase" ones (energy at zero abscissa). Given the off-minimum geometry of "solid-phase" fragments as compared to the "gas-phase" one, the global increase in HOMO energy indicates enhanced pi-conjugation efficiency in the "solid-phase", which is the expected result. On the other hand, Fig. 10 also shows several HOMO energies lying lower than the "gas-phase" one, indicating strong π-deconjugation. The overall distribution of the HOMO energies for each compound ($\Delta\varepsilon_{HOMO}$-geom) is thus a measure of the potential for a given molecule to undergo geometrical deformations under the influence of intermolecular interactions. This distribution can be estimated by calculating the differences between the largest- and the smallest HOMO energies for each compound. The calculated $\Delta\varepsilon_{HOMO}$-geom values are found to decrease in the order **4**(0.247 eV) > **7**(0.138 eV) > **5**(0.093 eV), with standard deviations following the same trend (Table 5). Plotting them as a function of the average dissociation

energies of compounds **4**, **5**, and **7** shows an excellent linear correlation (Fig. 11a), thus supporting the assumption for a *strong positive impact of the IE factor in the energetic disorder* in these compounds.

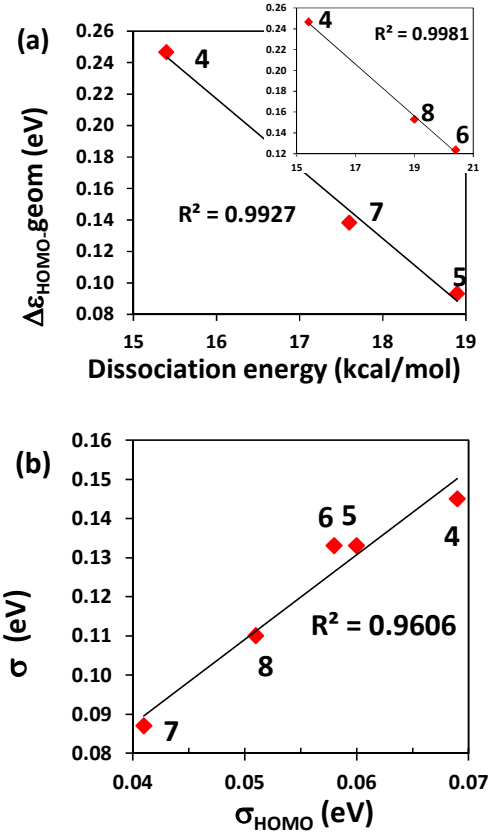

Fig. 11 (a) Width of HOMO energy distributions calculated for each isolated fragment ($\Delta\varepsilon_{HOMO}$-geom) in the six dimer types of compounds **4**, **5**, and **7**, parametric on the average dissociation energy over six dimers for each of compounds **4**, **5**, and **7** (**4**, **6**, and **8** in the inset). (b) Experimental σ values parametric on the standard deviation σ_{HOMO} of the HOMO energy distributions calculated for each fragment in the presence of the second fragment of the corresponding dimer, over six dimer types for each of compounds **4**, **5**, and **7**.

The above conclusion is supported by a global correlation between the trends in $\Delta\varepsilon_{HOMO}$-geom and the structural changes in compounds **4**, **5**, and **7**. Note that, in view of the HOMO distribution (Fig. 2 and S12) and the large degree of structural freedom in these compounds (Fig. 1), it is impossible to account for all geometrical changes. However, given the dominant contributions to HOMO of these compounds from the ethylenic- and surrounding phenyl moieties, we distinguish two main effects: (i) the change in the dihedral angle (Ph)C-C=C-C(Ph) between the two phenyl groups in *cis*-position around the ethylenic double bond (reported hereafter as dih-1), and (ii) the change in the dihedral angles between the ethylenic plane and the three surrounding phenyl groups (dih-2, average of three dihedral angles, each calculated over twelve different molecular geometries).

Our results indicate that the width of the distribution of dih-1 decreases in the order **4**(5.95°) > **7**(5.09°) ≈ **5**(5.05°). (ii) The width of distribution of dih-2 decreases by 5° in compound **5** as compared to **4** (24.1° and 29.1° respectively). Both effects correlate with the decreasing width of the HOMO energy distributions in the order **4** > **7** > **5**, and with the increasing intermolecular IE in the same order. Remembering that the increase in interaction energy in the order **4** < **7** < **5** is dominantly (60-70%) due to the additional H-bonds established by means of the methoxy and methyl groups (section 2.3), we conclude on the *direct correlation between the establishment of the H-bonds and the decrease of the geometrical randomness and the corresponding contribution to the energetic disorder*. The inset of Fig. 11a shows that the above conclusion remains unchanged if compounds **4**, **6**, and **8** are compared instead of **4**, **5**, and **7**. As for the difference between methoxy and methyl substitutions, Fig. 11a and Table 5 indicate that the difference between **5** and **7** is much smaller than between each of them and the unsubstituted compound **4**. Similarly, the differences in Table 5 between compounds **5** and **6** or between **7** and **8** are much smaller than between each of them and the unsubstituted compound **4**. *The impact of the nature of substitutions on the energetic disorder seems consequently of minor importance as compared to the impact of the IE factor*.

3.3 Impact of polarization: semi-quantitative estimations

Compared to the previous section, here we calculate the HOMO energy of a given fragment by a different method: for a given dimer, each fragment taken at the dimer geometry is calculated in the presence of the second dimer ("solid-phase", dashed lines in Fig. 10). This means that, with respect to the influence of the IE factor on the geometrical randomness, here we add the influence of the polarization due to the presence of the adjacent molecule. These results for the fragments were obtained by using the dimer Hamiltonians, which contain all attractive or repulsive terms related to the interaction with the second fragment of the corresponding dimer. While our analysis shows that the following results are pertinent, we are aware that the long-range polarization effects are absent, so that the results discussed in the following should be considered as semi-quantitative ones.

Table 5 Width of HOMO energy distributions (difference between maximum and minimum values) and their standard deviation over a distribution of 12 values, corresponding to the fragments involved in the six dimer types of compounds 4-8. Two series of values are presented, both being calculated for fragments taken at the dimer geometries. $\Delta\varepsilon_{HOMO}$-geom and σ_{HOMO}-geom correspond to calculations on isolated fragments (at the dimer geometry). In the case of $\Delta\varepsilon_{HOMO}$ and σ_{HOMO}, each fragment of a given dimer is calculated in the presence of the second fragment. All values are in eV.

Compound	4	5	6	7	8
$\Delta\varepsilon_{HOMO}$-geom	0.247	0.093	0.124	0.138	0.153
$\Delta\varepsilon_{HOMO}$	0.241	0.185	0.182	0.153	0.161
σ_{HOMO}-geom[a]	0.068*	0.034	0.041	0.041	0.051**

σ_{HOMO}[a]	0.069	0.060	0.058	0.043	0.050

[a] The Shapiro-Wilk normality tests at 5% threshold does not reject the Gaussian distribution hypothesis, except for (*), excluding only two values, and (**), not rejected only at the 1% threshold). See Table S10 for individual values of $\Delta\varepsilon_{HOMO}$.

Fig. 10 indicates a net difference between the two curves in the case of compound **5**, mainly indicating stabilization of HOMO levels due to the polarization effects. On the other hand, almost no difference can be observed for compound **7**, whereas a small destabilization can be observed in the case of compound **4**. This difference between the three compounds points to the difference in their dipole moments and/or in their dispersive/exchange interactions. However, our SAPT0 calculations on Dimer-6 for compounds **4**-**8** indicate that the sum of exchange and dispersion contributions (repulsive) in the intermolecular interaction energy increases only slightly (by 1.2 kcal/mol) between **4** and **6** (the weakest and the strongest interacting compounds), whereas the electrostatic and inductive contributions (both attractive) roughly increase in absolute values by 5.6 and 2.2 kcal/mol respectively in the order **4** < **7** < **8** < **5** < **6** (Table S8). The correlation with the increasing dipole moments in the same order seems consequently straightforward: in the balance between the attractive and repulsive terms impacting the HOMO energy, the attractive interactions seem to dominate in the case of compound **5**, very probably due to the large dipole moment (up to 3.8 D, Table 3). In the case of compound **7**, these interactions roughly cancel out (dipole moment 1.3 D), and become slightly repulsive in the case of compound **4** (dipole moment 0.8 D). The net result is that the width of the HOMO energy distribution for compound **5** increases importantly, yet remaining much smaller than that of compound **4**. This result is consistent with the minor role of σ_{dip} showed in Fig. 9 and Table 4, thus comforting the pertinence of our calculations.

The width of the HOMO energy distribution calculated by taking into account both the geometrical deformations (IE effect) and the (dipolar) polarization effects ($\Delta\varepsilon_{HOMO}$) thus varies in the order **4**(0.241 eV) > **5**~**6**(0.185 and 0.182 eV) > **8**(0.161 eV) > **7**(0.153 eV), with standard deviations following the same trend (σ_{HOMO} in Table 5). Due to the presence of the electrostatic effects in the calculated $\Delta\varepsilon_{HOMO}$ values, we compare their trend with the trend of the experimental σ values (0.145, 0.133, 0.133, 0.110, and 0.087 eV, for **4**, **5**, **6**, **8**, and **7** respectively, Table 4). Interestingly, both trends are quite similar, again comforting the pertinence of this model. This conclusion seems to be reinforced by a good linear correlation between the experimental σ and theoretical σ_{HOMO} (Fig. 11b).

Intriguingly, the calculated σ_{HOMO} values are smaller by roughly two times as compared to the experimental σ. As mentioned previously, (i) this may be due to the limited model applied here (absence of long-range polarization contributions and intermolecular structural randomness). We speculate that the effect of H-bonds (IE factor in general) in the intermolecular structural randomness across the series **4**-**8** is expected to follow the same trend as the intramolecular structural randomness, which we "explain" with the enhanced occurrence of the stronger interacting (H-bond oriented) dimer-types as compared to the weakest ones. (ii) Other factors may be in play (see next section).

We finally highlight that, in line with TOF measurements and σ_{dip} determinations (Table 4), the effect of the dipole moments in the trends in $\Delta\varepsilon_{HOMO}$ or in σ_{HOMO} values is found to influence only the order between the methoxy and methyl substituted compounds, leaving unchanged the trends between the substituted- (**5**-**8**) versus unsubstituted (**4**) ones. Comparing compounds **5**-**8** as a single block with respect to compound **4**, we again conclude that *the positive effect of the IE factor on the energetic disorder in compounds **5**-**8** is dominant over the effect of the dipole moments*.

3.4 Methoxy versus methyl substitutions: influence of softness and conformational freedom.

In the previous section we showed that the large dipole moments of compounds **5** and **6** were in the origin of their larger energy disorder as compared to the methyl substituted compounds **7** and **8**. We suggest that additional factors accounting for the larger width of the DOS of methoxy-versus-methyl substituted compounds may include:

(i) additional conformational freedom of the methoxy groups around the C-O bonds (compounds **5**-**6**) as compared to the methyl substituents (**7**-**8**). This is expected to induce two negative effects to the polarization distribution: firstly, compared to a given random intermolecular geometry, the random orientation of methoxy groups is expected to result in additional intermolecular orientations, hence in *increase of the intermolecular positional (polarization) randomness*. Secondly and very importantly, the random orientation of methoxy groups *increases the distribution of dipole moment values* (0.8-3.8 D, Table 3), due to the random orientation of the local C-O dipole moments.

The impact of these two negative effects is expected to increase with the number of molecular conformations. Fig. 12a shows the evolution of σ_{vdW} values of compounds **5**-**8** parametric in log(N), with N being the number of additional conformers associated with the presence of methyl or methoxy groups (Table 4). A global increase of σ_{vdW} values with log(N) can be observed, which seems to support the above assumption. Interestingly, different degrees of conformational freedom in polymer chains have been previously found to explain differences in their σ values.[23]

(ii) *The larger propensity to polarization* of the methoxy substituted compounds as compared to the methyl case. Generally, this intrinsic molecular property characterizes the degree to which the electronic cloud of a given molecule will be distorted due to the electric field created by the nearby charges or multipoles (permanent or induced). Compared to a "hard" molecule, an easily polarizable electronic cloud of a "soft" molecule is more responsive to randomly distributed charges and multipoles, thus giving rise to a larger distribution of site energies, hence larger σ values. As a means to check for this effect in the case of our compounds, we have calculated the static isotropic polarizabilities of compounds **4**-**8**. The results shown in Table 3 indicate increasing molecular

polarizabilities in the order **4** < **7** < **8** < **5** < **6**. Limiting the comparison to compounds **5**-**8**, increasing σ_{vdW} in the same order is consequently expected, which is indeed what is shown in Fig. 12b.[24]

Both factors mentioned here, along with the impact of the dipole moments discussed in the previous section, allow explaining for (i) the larger σ and σ_{vdW} values of methoxy-substituted compounds as compared to the methyl-substituted ones, and (ii) the increase in σ and σ_{vdW} values of **6** as compared to **5** and of **8** as compared to **7**.

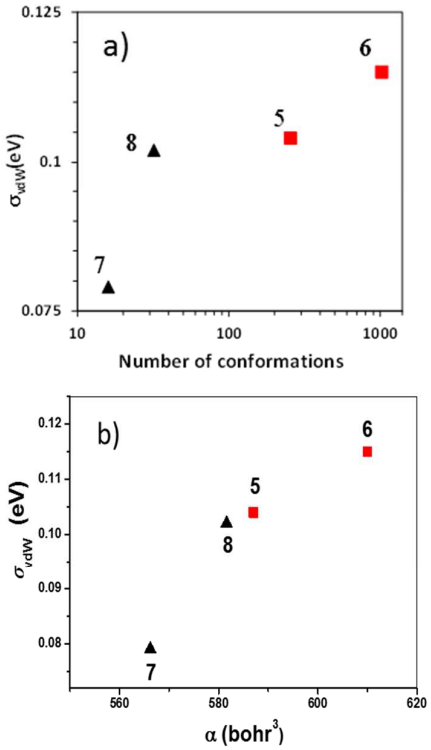

Fig. 12 (a) σ_{vdW} values of compounds **5**-**8** parametric in log(N). N is the number of additional conformers associated with the presence of methyl or methoxy groups. (b) σ_{vdW} parametric on the static isotropic polarizability of compounds **4**-**8**.

3.5 Relative importance of different factors

Resuming the above analysis, we suggest that the width of the DOS in these compounds results from a delicate balance between (at least) four components: (i) the polarization distribution due to the geometrical randomness, which is controlled by the IE factor, (ii) the polarization distribution due to the permanent dipole moments, (iii) the polarization distribution related to the conformational degree of freedom, and (iv) the intrinsic molecular polarizability of the electronic clouds. Across the series of compounds **4**-**8**, these factors play in opposite senses: while the IE factor contributes to decrease the polarization distribution by means of the reduced structural randomness (**5**-**8** as compared to **4**), the increase in intrinsic molecular polarizability (**5**-**8**), in dipole moments (**5**-**8**), and in conformational freedom (**5**-**6**) play in the opposite sense. The smaller σ and σ_{vdW} values of compounds **5**-**8** as compared to **4** suggest that, *in the balance between these four contributions, the IE factor is dominant*; that is to say, the geometrical randomness due to loosely interacting molecules is the main source of disorder in compound 4. This last conclusion is also supported by (i) the larger decrease in σ^2_{vdW} between **4** and **5** (47%, Table 4) or between **4** and **7** (71%), as compared to the difference between **5** and **6** (12%), **5** and **7** (24%), or between **7** and **8** (23%). (ii) the minor effect of dipole moments deduced from the trends in $\Delta\varepsilon_{HOMO}$ and σ_{HOMO} values.

The large hole-mobility found for the methyl substituted compounds thus stems from a judicious tuning of the delicate balance between the above factors: moderate increase in the dipole moments, in the molecular softness, and in the conformational freedom, while simultaneously and non-negligibly increasing the intermolecular interaction energy.

Experimental Section

Instrumentation

^{1}H NMR and ^{13}C NMR spectra were obtained of the solutions in deuterated chloroform with a Varian Unity Inova spectrometer. IR spectroscopy was performed with Perkin Elmer Spectrum GX II FT-IR System using KBr pallets. Mass spectra were obtained on a Waters ZQ 2000 mass spectrometer. Elemental analysis was performed with an Exeter Analytical CE-440 Elemental Analyser. Thermogravimetric analysis (TGA) was performed on Mettler TGA/SDTA851e/LF/1100 apparatus at a heating rate of 20 ºC/min under nitrogen atmosphere. Differential scanning calorimetry (DSC) measurements were performed on DSC Q 100 TA Instrument at a heaing/cooling rate of 10 ºC/min under nitrogen atmosphere. Absorption and fluorescence spectra of 10^{-4} M solutions in tetrahydrofuran of the synthesized compounds were recorded in quartz cells using a Perkin Elmer Lambda 35 spectrometer and Hitachi MPF-4 spectrofluorophotometer respectively. Cyclic voltammetry (CV) measurements were carried in a three electrode cell using platinum rod as a counter electrode, glassy carbon as working electrode and $Ag/AgNO_3$ as the reference electrode. The experiments were carried out in dry dichloromethane solution containing 0.1 M tetrabutylammonium perchlorate as electrolyte at room temperature under nitrogen atmosphere at a scan rate 50 mV/s. The measurements were calibrated using the internal standard ferrocene/ferrocenium (Fc/Fc^+).

The ionization potentials (IP_{PE}) of the films of the synthesized compounds were measured by the electron photoemission in air method.[25] The samples for the ionization potential measurements were prepared by dissolving compounds in THF and coated onto Al plates pre-coated with 0.5 µm thick adhesive layer of the copolymer of methylmethacrylate and methacrylic acid (MKM). The function of this layer was not only to improve adhesion but also to eliminate electron photoemission from Al.

Hole-drift mobility of the materials was estimated by a time-of-flight (TOF) method. The samples were fabricated with structures of ITO/compound/Al. Commercial indium tin oxide

(ITO) coated glass was used as a substrate, which was first cleaned chemically using a bath of distilled water and acetone. Organic and aluminum films were sequentially vacuum-deposited onto precleaned ITO-coated glass substrates under the vacuum of $2\text{-}5\cdot10^{-6}$ mBar using vacuum equipment from Kurt J. Lesker in-built in an MB EcoVap4G glove box. In the ToF experiments, charges were generated by a pulsed third-harmonic Nd:YAG laser EKSPLA NL300 working at a pulse duration of 3-6 ns and the wavelength of 355 nm. Electric fields were applied by a Keithley 6517B electrometer. A digital storage oscilloscope Tektronix TDS 3032C was used to record ToF transients. The drift mobility was calculated by using the formula $\mu=d^2/U\cdot t_{tr}$, where d is the layer thickness, and U the surface potential at the moment of illumination, and t_{tr} is the transit time which was taken from the TOF transients.

Additional details on the TOF data processing are given in Annex I.

Materials

The starting compounds 4,4'-diaminobenzophenone, iodobenzene, 4-iodanisole, 4-iodotoluene, diethyl benzylphosphonate, diethyl-4-methylbenzylphosphonate, diethyl 4-methoxybenzylphosphonate and the required chemicals, i.e. copper powder, 18-crown-6 (Aldrich), *o*-dichlorobenzene (all from Aldrich), potassium carbonate (Eurochemicals), potassium *tert*-butoxide (Aldrich), anhydrous sodium sulfate (Eurochemicals) were purchased as reagent grade chemicals and used as received.

General procedure for the synthesis of compounds 1-3 by Ullmann reaction

4,4'-Diaminobenzophenone (2 g, 9.4 mmol) was dissolved in *o*-dichlorbenzene (20 ml) with iodobenzene (11.5 g, 56.5 mmol), 4-iodanisole (13.2 g, 56.5 mmol) or 4-iodotoluene (12.3 g, 56.5 mmol). Copper powder (2.4 g, 37.7 mmol), 18-crown-6 (0.5 g, 1.9 mmol) and potassium carbonate (10.4 g, 75.4 mmol) were added to the solution. The reaction mixture was stirred at 180 ºC under argon atmosphere. After 24 h the inorganic components were removed by filtration of the hot mixture. The solvent was removed by distillation under reduced pressure.

Bis(4-(diphenylamino)phenyl)methanone (**1**): The compound was purified by column chromatography using ethyl acetate and hexane in a volume ratio of 1:5 as an eluent. The yield of **1** yellow solid was 3.8 g (78 %), mp 187-188 ºC, lit.[26] 188-189 ºC. IR (KBr), ν/cm^{-1}: 3036, 3059 (ar. C-H), 1489, 1586 (ar. C=C), 1648 (C=O), 1276, 1311, 1325 (C-N). ^{1}H NMR (300 MHz, $CDCl_3$-d_6, δ): 7.02 (d, 4H, *J*=9.14 Hz, Ar), 7.09-7.18 (m, 12H, Ar), 7.28-7.34 (m, 8H, Ar), 7.68 (d, 4H, *J*=9.16, Ar). ^{13}C NMR (75 MHz, $CDCl_3$-d_6, δ): 120.19, 124.63, 126.05, 129.81, 130.83, 131.85, 146.96, 151.65, 194.19. MS ($APCl^+$), *m/z* =517 [M^+].

Bis(4-(bis(4-methoxyphenyl)amino)phenyl)methanone (**2**): The compound was purified by column chromatography using ethyl acetate and hexane in a volume ratio of 1:3 as an eluent. The yield of **2** yellow solid was 4.8 g (81 %). IR (KBr), ν/cm^{-1}: 3040 (ar. C-H), 2931, 2952, 2997, (aliph. C-H), 2833 (O-CH_3), 1440, 1505, 1593 (ar. C=C), 1643 (C=O), 1272, 1286, 1271 (C-N), 1243 (C-O-C). ^{1}H NMR (300 MHz, $CDCl_3$-d_6, δ): 3.81 (s, 12H, OCH_3), 6.83-6.88 (m, 12H, Ar), 7.12 (d, 8H, *J*=9.16, Ar), 7.63 (d, 4H, *J*=9.16, Ar). ^{13}C NMR (75 MHz, $CDCl_3$-d_6, δ): 55.47, 114.87, 117.04, 127.66, 129.09, 131.65, 139.53, 151.98, 152.00, 156.74, 193.76. MS ($APCl^+$), *m/z* =637 [M^+].

Bis(4-(bis(4-methylphenyl)amino)phenyl)methanone (**3**): The compound was purified by column chromatography using THF and hexane in a volume ratio of 1:6 as an eluent. The yield of **3** yellow solid was 3.8 g (72 %). IR (KBr), ν/cm^{-1}: 3025, 3058 (ar. C-H), 2860, 2919, 2945, (aliph. C-H), 1507, 1594 (ar. C=C), 1647 (C=O), 1276, 1294, 1318 (C-N). ^{1}H NMR (300 MHz, $CDCl_3$-d_6, δ): 2.33 (s, 12H, CH_3), 6.94 (d, 4H, *J*=8.74, Ar), 7.04-7.13 (m, 16H, Ar), 7.64 (d, 4H, *J*=8.73, Ar). ^{13}C NMR (75 MHz, $CDCl_3$-d_6, δ): 21.18, 118.99, 126.17, 130.11, 130.42, 131.82, 134.42, 144.38, 151.90, 194.13. MS ($APCl^+$), *m/z* =573 [M^+].

General procedure for the synthesis of compounds 4-8 by Wittig-Horner reaction.

Ketone **1** (1 g, 1.9 mmol), **2** (1 g, 1.8 mmol) or **3** (1 g, 1.6 mmol) and the corresponding benzylphosphonate (2 molar equivalents) were dissolved in anhydrous THF. Potassium *tert*-butoxide (4 molar equivalents) was added slowly to the solution at room temperature under argon atmosphere. The reaction mixture was stirred for 1 h. After completion (TLC monitoring), the reaction mixture was diluted with water and extracted with ethyl acetate. The organic layer was dried over anhydrous sodium sulfate. The solvent was removed by distillation.

4,4'-(2-Phenylethene-1,1-diyl)bis(N,N-diphenylaniline) (**4**): The product was purified by column chromatography using ethyl acetate and hexane in a volume ratio of 1:10 as an eluent. The yield of **4** yellow crystals was 0.5 g (43 %), mp 154-155 ºC, lit.[23] 154-156 ºC. IR (KBr), ν/cm^{-1}: 3032, 3059 (ar. C-H), 1490, 1507, 1586 (ar. C=C), 1313, 1322, 1325 (C-N). ^{1}H NMR (300 MHz, $CDCl_3$-d_6, δ): 6.89 (s, 1H, CH), 6.98-7.18 (m, 23H, Ar), 7.23-7.28 (m, 10H, Ar). ^{13}C NMR (75 MHz, $CDCl_3$-d_6, δ): 123.11, 123.28, 123.99, 124,60, 124.81, 126.70, 128.15, 128.58, 129.52, 129.77, 131.60, 134.61, 137.29, 138.06, 142.09, 147.24, 147.58, 147.86, 147.93. MS ($APCl^+$), *m/z* =591 [M^+]. Anal. Calcd. for $C_{44}H_{34}N_2$: C 89.46; H 5.80; N 4.74. Found: C 89.47; H 5.78; N 4.75.

4,4'-(2-Phenylethene-1,1-diyl)bis(N,N-bis(4-methoxyphenyl)aniline) (**5**): The product was purified by column chromatography using acetone and hexane in a volume ratio of 1:8 as an eluent. The yield of **5** yellow crystals was 0.6 g (55 %), mp 176-177 ºC. IR (KBr), ν/cm^{-1}: 3007, 3038 (ar. C-H), 2900, 2929, 2943 (aliph. C-H), 2832 (O-CH_3), 1442, 1461, 1505, 1598 (ar. C=C), 1278, 1319 (C-N), 1239 (C-O-C). ^{1}H NMR (300 MHz, $CDCl_3$-d_6, δ): 3.79 (s, 12H, OCH_3), 6.81-6.88 (m, 13H, Ar), 6.99 (d, 2H, *J*=8.71, Ar), 7.05-7.08 (m, 10H, Ar), 7.13-7.20 (m, 5H, Ar). ^{13}C NMR (75 MHz, $CDCl_3$-d_6, δ): 55.75, 114.90, 114.92, 120.08, 120.80, 125.65, 126.36, 126.71, 126.89, 128.08, 128.44, 129.66, 131.13, 132.61, 135.67, 138.42, 141.07, 141.23, 148.06, 155.96, 156.12. MS ($APCl^+$), *m/z* =711 [M^+]. Anal. Calcd. for $C_{45}H_{36}N_2O$: C 87.06; H 5.85; N 4.51; O 2.58. Found: C 87.09; H 5.83; N 4.50.

4,4'-(2-(4-Methoxyphenyl)ethene-1,1-diyl)bis(N,N-bis(4-methoxyphenyl)aniline) (**6**): The product was purified by column chromatography using ethyl acetate and hexane in a volume ratio of 1:8 as an eluent. The yield of **6** yellow solid

was 0.6 g (52 %). IR (KBr), ν/cm^{-1}: 3035 (ar. C-H), 2905, 2931, 2950, 2997 (aliph. C-H), 2833 (O-CH_3), 1440, 1463, 1505, 1605 (ar. C=C), 1283, 1318 (C-N), 1240 (C-O-C). ^{1}H NMR (400 MHz, $CDCl_3$-d_6, δ): 3.81 (s, 3H, OCH_3), 3.82 (s, 12H, OCH_3), 6.73 (d, 2H, *J*=8.77, Ar), 6.80 (s, 1H, CH), 6.84-6.92 (m, 12H, Ar), 7.02-7.05 (m, 4H, Ar), 7.08-7.11 (m, 8H, Ar), 7.19 (d, 2H, *J*=8.72, Ar). ^{13}C NMR (101 MHz, $CDCl_3$-d_6, δ): 55.21, 55.51, 113.31, 114.65, 120.00, 120.67, 125.02, 126.46, 126.58, 127.97, 130.61, 130.88, 131.08, 135.72, 140.23, 140.90, 141.01, 147.67, 147.92, 155.70, 155.81, 157.93. MS (APCl$^+$), *m/z* =741 [M$^+$]. Anal. Calcd. for $C_{49}H_{44}N_2O_5$: C 79.44; H 5.99; N 3.78; O 10.80. Found: C 79.48; H 5.97; N 3.79.

4,4'-(2-Phenylethene-1,1-diyl)bis(N,N-bis(4-methylphenyl)aniline) (**7**): The product was purified by column chromatography using ethyl acetate and hexane in a volume ratio of 1:20 as an eluent. The yield of **7** was 0.4 g (39 %). IR (KBr), ν/cm^{-1}: 3027, 3059 (ar. C-H), 2855, 2920, 2952 (aliph. C-H), 1502, 1594 (ar. C=C), 1275, 1322 (C-N). ^{1}H NMR (300 MHz, $CDCl_3$-d_6, δ): 2.32 (s, 12H, CH_3), 6.86 (s, 1H, CH), 6.95-7.10 (m, 22H, Ar), 7.12-7.25 (m, 7H, Ar). ^{13}C NMR (101 MHz, $CDCl_3$-d_6, δ): 20.81, 121.74, 122.61, 124.55, 124.78, 125.93, 126.25, 127.83, 128.19, 129.46, 129.84, 129.88, 131.16, 132.65, 133.48, 136.28, 138.04, 142.05, 145.16, 145.28, 147.26, 147.70.MS (APCl$^+$), *m/z* =647 [M$^+$]. Anal. Calcd. for $C_{45}H_{36}N_2$: C 89.37; H 6.00; N 4.63. Found: C 89.33; H 6.02; N 4.65.

4,4'-(2-(4-Methylphenyl)ethene-1,1-diyl)bis(N,N-bis(4-methylphenyl)aniline) (**8**): The product was purified by column chromatography using ethyl acetate and hexane in a volume ratio of 1:20 as an eluent. The yield of **8** yellow solid was 0.5 g (40 %). IR (KBr), ν/cm^{-1}: 3026, 3058, 3078 (ar. C-H), 2856, 2919, 2951 (aliph. C-H), 1506, 1592 (ar. C=C), 1272, 1321 (C-N). ^{1}H NMR (300 MHz, $CDCl_3$-d_6, δ): 2.29, (s, 3H, CH_3), 2.31 (s, 12H, CH_3), 6.82 (s, 1H, CH), 6.93-7.08 (m, 26H, Ar), 7.21 (d, 2H, *J*=8.73 Hz, Ar). ^{13}C NMR (75 MHz, $CDCl_3$-d_6, δ):.21.08, 21.46, 122.09, 122.95, 124.78, 124.98, 126.19, 128.33, 128.86, 129.62, 130.10, 130.12, 131.38, 132.63, 132.83, 135.98, 135.37, 136.29, 136.72, 141.36, 145.43, 145.56, 147.48, 147.78. MS (APCl$^+$), *m/z* =661 [M$^+$]. Anal. Calcd. for $C_{49}H_{44}N_2$: C 89.05; H 6.71; N 4.24. Found: C 89.38; H 5.98; N 4.64.

Computational methodology

DFT[27] calculations employing the B3LYP[28,29], ωB97X-D[30], and LC-ωPBE[31,32] functionals were performed with the Gaussian 09 program[33] The geometry optimizations for all the molecules were carried out without symmetry constraints by using the 6-31G(d,p) basis set, followed by frequency calculations. The geometry optimizations of the cationic radical species were performed at the restricted open shell level.

The spectroscopic properties of the molecules were calculated by mean of time dependent density functional theory method (TDDFT)[34-38] with the 6-31G(d,p) basis set. Up to 20 excited states were calculated and the theoretical absorption bands were obtained by considering a band half-width at half-maximum of 0.2 eV.[39] Excited state dipole moments were roughly estimated by performing triplet-state single-point calculations at the geometry of the ground state.

The vertical ionization potentials (IP) were calculated at the B3LYP/6-31G(d,p) level as energy difference between neutral and cation radical species at the neutral state geometry.

The internal reorganization energies (λ_i) were calculated with the 6-31G(d,p) basis set by mean of the following equation:[40]

$$\lambda_i = \lambda_i^1 + \lambda_i^2 = (E_M^{G-M^+} - E_M^{G-M}) + (E_{M^+}^{G-M} - E_{M^+}^{G-M^+}) \quad (2)$$

In this equation the quantity $E_M^{G\text{-}M+}$ for instance corresponds to the energy of the neutral molecule (*M)* in the geometry of the cationic species (M^+).

In order to correctly describe the π-stacking interactions, the geometries of selected model dimers formed by two identical molecules of each compound have been optimized by employing the ωB97X-D[30] functional at the 6-31G(d,p) basis set. Previous studies have shown that this functional provides good results on the description of weak interactions.[41,42] The dimer reported as "Dimer type 6" is similar to one of dimer-types extracted from the crystal structure (see Fig. S1 and S2) corresponding to the largest spatial overlap between adjacent molecules. In the case of methoxy and methyl substituted compounds **5**-**8**, identical dimer-types with those of compound **4** were considered by appropriate substitutions in the optimized dimer geometries of compound **4**. The optimized Cartesian coordinates of Dimer-6 of compounds **4**-**8** are given in Annex III. The relative dissociation energy (ΔE_D) between for instance, the methoxy substituted compound **5** with respect to **4** was calculated by firstly calculating the ΔE_D between dimer-isomers of identical type (six ΔE_D calculated for the six dimer-isomers of compounds **4** and **6**), and subsequently calculating the average value of the six ΔE_D values.

The interaction energies of the optimized model dimers were calculated by applying two different approaches: (i) with respect to the isolated monomers at the ωB97XD/6-31G(d,p) level in gas phase, including corrections for the basis set superposition error (BSSE) computed by the counterpoise correction method of Boys and Bernardi.[43] The zero point energy (ZPE) correction has been also taken into account. (ii) by means of SAPT[44] calculations at the SAPT0/jun-cc-pvdz level, also allowing for energy decomposition analysis (Annex II, SI). We note that the trends in the interaction energies across the series of compounds **4**-**8** are identical in both approaches.

The electronic couplings between the HOMO orbitals of two adjacent molecules were calculated at the B3LYP/ 6-31G(d,p) level, according to the approach described by Valeev et al.[45] with the corresponding matrix elements evaluated with Gaussian 09.

Finally, the dipole component σ_{dip} values of the energetic disorder for the model compounds were estimated based on the Dieckmann's[20] and Yang's[21] relation:

$$\sigma_{dip} = \frac{k_0 c^n p}{d^2 \varepsilon} \quad (3)$$

In this equation, *c* is the fraction of lattice sites occupied by the molecules (1 in the case of our pure film compounds), *p* is the dipole moment, *d* is the distance between two charge-transport molecules (in Å), ε is the relative dielectric constant. Values of k_0 =3.06 and n =2/3 (according to Dieckmann) were used in our estimations. The dipole moment of methoxy

substituted compounds range between 0.8-3.8 Debye and 1.1-3.3 Debye for the compounds **5** and **6** respectively, so average *p* values (2.8 Debye and 2.2 Debye for the compounds **5** and **6** respectively) were considered in Equation 2. As for the intermolecular distance (*d)*, average values over six optimized dimers were considered for each model compound. The dielectric constant was considered to be identical for all compounds (ε=3). We underline that the pertinent parameter used in the discussions (Table 4 and Section 3) is the % σ_{dip} value with respect to the total σ value. Decreasing the ε value of compound 4 (the less polar compound) from 3 to 2 results in increase of the % σ_{dip} value from 3% to 7%, whereas increasing the ε value from 3 to 4 results in decreased % σ_{dip} values for all compounds. The dominant contribution of the van der Waals term (Table 4 and Section 3) and all the conclusions based on this comparison remain consequently independent from the choice of the ε value.

Conclusions

The new triphenylamine-twin compounds presented in this study exhibited high thermal stability and formed glasses with glass transition temperatures ranging from 71 to 77 °C. The derivatives having methoxy groups show the lowest ionization potentials. Good hole-drift mobilities were observed across the series of these compounds, exceeding 10^{-2} cm^2/Vs for the compounds containing methyl groups.

The hole transport properties of compounds **4**-**8** are dominated by disorder phenomena, exhibiting decreasing energetic disorder parameter σ upon substitutions in the order H > OCH_3 > CH_3. The dipole moments increase importantly upon substitution (by up to 2-3D) in the order H < CH_3 < OCH_3, yet the σ_{dip} contributions remain of minor importance (3-39%) as compared to the van der Waals component (σ_{vdW}). The decreasing σ upon substitutions is due to the strong decrease in van der Waals component (σ_{vdW}), which counterbalances the increasing dipolar component (σ_{dip}). It is thus important to highlight that increasing the dipole moment of the molecules is not necessarily synonym of decrease in charge mobility.

Amongst others, four factors impacting the width of the DOS in compounds 4-8 were discussed here: the interaction energy between adjacent molecules, the presence of permanent dipole moments, the conformational degree of freedom, and molecular polarizability. These factors are in competition: the increase in intermolecular IE tends to decrease the σ_{vdW} (and σ) values, whereas the increase in dipole moments, in conformational degree of freedom, and in molecular polarizability result in increasing disorder. Our results indicate that among these factors, the dominant consequence of methoxy and methyl substitutions in compound **4** is the decrease in geometrical disorder due to the enhancement of the intermolecular interactions, principally due to the potential of these groups to establish efficient hydrogen-bonds. We assume the hydrogen bonds to behave as efficient anchor arms between adjacent molecules, thus being in the origin of the reduced structural and polarization randomness of the substituted compounds **5**-**8** as compared to the non-substituted one. To the best of our knowledge, the above correlation between the potential of methoxy and methyl groups to strengthen the intermolecular interactions via H-bonds, and the decrease in σ and σ_{vdW} values, is a new aspect not yet discussed in the literature.

Acknowledgements

This work has been financially supported by the Taiwan-Latvia-Lithuania cooperation project "Synthesis and studies of organic electroactive materials for effective and reliable optoelectronic devices" (TAPLLT1/13). G.S. acknowledges the calculation centre of Cergy-Pontoise University for the computer time support, V. Coropceanu and B. Kippelen (Georgia Tech', Atlanta, Georgia, USA), and M.K. Ravva (KAUST, Saudi Arabia) for stimulating discussions.

Notes and references

1 C. Ruiz, E. M. Garcia-Frutos, G. Hennrich, B. Gomez-Lor, *J. Phys. Chem. Lett.,* 2012, **3**, 1428.
2 S. R. Forrest, M. E. Thompson, *Chem. Rev*., 2007, **107**, 923.
3 K. Walzer, B. Maennig, M. Pfeiffer, K. Leo, *Chem. Rev.,* 2007, **107**, 1233.
4 Y. Shirota, H. Kageyama, *Chem. Rev.,* 2007, **107**, 953.
5 P. Strohriegl, J. V. Grazulevicius, *J. Adv. Mater*., 2002, **14**, 1439.
6 P. M. Borsenberger, E. H. Magin, M. B. Oregan, J. A. Sinicropi. *J. Polym. Sci., Part B: Polym. Phys.,* 1996, **34**, 317.
7 J. L. Maldonado, M. Bishop, C. Fuentes-Hernandez, P. Caron, B. Domercq, Y. D. Zhang, S. Barlow, S. Thayumanavan, M. Malagoli, J. L. Bredas, S. R. Marder, B. Kippelen, *Chem. Mater.,* 2003, **15**, 994.
8 T. Malinauskas, M. Daskeviciene, G. Bubniene, I. Petrikyte, S. Raisys, K. Kazlauskas, V. Gaidelis, V. Jankauskas, R. Maldzius, S. Jursenas, V. Getautis, *Chem. Eur. J.,* 2013, **19**, 15044.
9 D. Gudeika, J. V. Grazulevicius, G. Sini, A. Bucinskas, V. Jankauskas, A. Miasojedovas, S. Jursenas, *Dyes and Pigments*, 2014, **106**, 58.
10 J. Keruckas, R. Lygaitis, J. Simokaitiene, J. V. Grazulevicius, V. Jankauskas, G. Sini, *J. Mater. Chem.,* 2012, **22**, 3015.
11 M. Nishio, *Kagaku no Ryoiki,* 1977, **31**, 834.
12 Y. Kodama, K. Nishihata, M. Nishio, N. Nakagawa, *Tetrahedron Lett.,* 1977, 2105.
13 M. Nishio, *PCCP* 2011, **13**, 13873.
14 R. A. Marcus, *J. Chem. Phys.,* 1956, **24**, 966.
15 R. A. Marcus, *Reviews of Modern Physics,* 1993, **65**, 599.
16 R. A. Marcus, N. Sutin, *Biochim. Biophys. Acta,* 1985, **811**, 265.
17 K. Xu, F. Zhang, X. Zhang, Qi. Hu, H. Wu, and S. Guo. *J. Mater. Chem. A*, 2014, **2**, 8545.
18 P. M. Borsenberger, W. T. Gruenbaum, E. H. Magin, L. J. Sorriero, *Chem. Phys.,* 1995, **195**, 435.
19 H. Bassler, Physica Status Solidi B - Basic Research, 1993, **175**, 15.
20 A. Dieckmann, H. Bassler, P. M. Borsenberger, *J. Chem. Phys.,* 1993, **99**, 8136.
21 R. H. Young, Philosophical Magazine B - Physics of Condensed Matter Statistical Mechanics Electronic Optical and Magnetic Properties, 1995, **72**, 435.
22 P.M. Borsenberger and H. Bassler, *J. Chem. Phys,.* 1991, **95**, 5327.
23 S.T. Hoffmann, H. Bassler, A. Kohler, *J. Phys. Chem. B,* 2010, **114**, 17037.

24 The increasing polarizability in the order **4** < **7** < **8** < **5** < **6** could be considered as due to the increasing number of electrons in the same order. However, by subtracting the contribution of the substituents (R=H, CH_3, OCH_3) from the total polarizability values, we have estimated the polarizability of the core-compounds, corresponding to the same number of electrons for each compound (**Table 3**). Similar trend in polarizabilities is obtained.

25 E. Miyamoto, Y. Yamaguchi, M. Yokoyama, *Electrophotography*., 1989, **28**, 364.

26 M. Plater, T. Jackson, *Tetrahedron*., 2003, **59**, 4673.

27 W. Kohn, L. Sham, *J. Phys. Rev.,* 1965, **140**, A1133.

28 C. T. Lee, W. T.Yang, R. G. Parr, *Phys. Rev. B,* 1988, **37**, 785.

29 A. D. Becke, *J. Chem. Phys.* 1993, **98**, 5648.

30 J. D. Chai, M. Head-Gordon, *Phys. Chem. Chem. Phys.,* 2008, **10**, 6615.

31 O. A. Vydrov, J. Heyd, A. V. Krukau, G. E. Scuseria, *J. Chem. Phys.,* 2006, **125**, 074106.

32 O. A. Vydrov, G. E. Scuseria, *J. Chem. Phys.,* 2006, **125**, 234109.

33 M. J. Frisch, G. W. Trucks, H. B. Schlegel, G. E. Scuseria, M. A. Robb, J. R. Cheeseman, G. Scalmani, V. Barone, B. Mennucci, G. A. Petersson, H. Nakatsuji, M. Caricato, X. Li, H. P. Hratchian, A. F. Izmaylov, J. Bloino, G. Zheng, J. L. Sonnenberg, M. Hada, M. Ehara, K. Toyota, R. Fukuda, J. Hasegawa, M. Ishida, T. Nakajima, Y. Honda, O. Kitao, H. Nakai, T. Vreven, J. J. A. Montgomery, J. E. Peralta, F. Ogliaro, M. Bearpark, J. J. Heyd, E. Brothers, K. N. Kudin, V. N. Staroverov, T. Keith, R. Kobayashi, J. Normand, K. Raghavachari, A. Rendell, J. C. Burant, S. S. Iyengar, J. Tomasi, M. Cossi, N. Rega, J. M. Millam, M. Klene, J. E. Knox, J. B. Cross, V. Bakken, C. Adamo, J. Jaramillo, R. Gomperts, R. E. Stratmann, O. Yazyev, A. J. Austin, R. Cammi, C. Pomelli, J. W. Ochterski, R. L. Martin, K. Morokuma, V. G. Zakrzewski, G. A. Voth, P. Salvador, J. J. Dannenberg, S. Dapprich, A. D. Daniels, O. Farkas, J. B. Foresman, J. V. Ortiz, J. Cioslowski, D. J. Fox, 2009, *Gaussian 09, Revision B.01, Gaussian Inc., Wallingford CT,* 2010.

34 E. K. U. Gross, W. Kohn, *Phys. Rev. Lett.,* 1985, **55**, 2850.

35 E. Runge, E. K. U. Gross, *Phys. Rev. Lett.,* 1984, **52**, 997.

36 E. K. U. Gross, W. Kohn, *Adv. Quant. Chem.,* 1990, **21**, 255.

37 R. Bauernschmitt, R. Ahlrichs, *Chem. Phys. Lett.,* 1996, **256**, 454.

38 M. E. Casida, C. Jamorski, K. C. Casida, D. R. Salahub, *J. Chem. Phys.,* 1998, **108**, 4439.

39 V. GaussView, R. Dennington, T. Keith, J. Millam, *Inc. Semichem, Shawnee Mission KS,* 2009.

40 J. L. Bredas, D. Beljonne, V. Coropceanu, J. Cornil, *Chem. Rev.*, 2004, **104**, 4971.

41 G. Sini, J. S. Sears, J. L. Bredas, *J. Chem. Theory Comput.,* 2011, **7**, 602.

42 S. N. Steinmann, C. Piemontesi, A. Delacht, C. Corminboeuf, *J. Chem. Theory Comput.,* 2012, **8**, 1629.

43 S. F. Boys, F. Bernardi, *Mol. Phys.,* 1970, **19**, 553.

44 J. M. Turney, A. C. Simmonett, R. M. Parrish, E. G. Hohenstein, F. Evangelista, J. T. Fermann, B. J. Mintz, L. A. Burns, J. J. Wilke, M. L. Abrams, N. J. Russ, M. L. Leininger, C. L. Janssen, E. T. Seidl, W. D. Allen, H. F. Schaefer, R. A. King, E. F. Valeev, C. D. Sherrill, T. D. Crawford, *WIREs Comput. Mol. Sci.,* 2012, **2**, 556.

45 E. F. Valeev, V. Coropceanu, D. A. da Silva, S. Salman, J. L. Bredas, *J. Amer. Chem. Soc.,* 2006, **128**, 9882.

GRAPHICAL ABSTRACT

Hole-transporting triphenylamine-based derivatives containing methoxy and methyl groups exhibit hole mobility reaching 10^{-2} cm^2/Vs. The potential of the methoxy and methyl groups to improve the hole mobility via hydrogen bonds is showed.